Mössbauer effect studies of $Fe_{100-x}Ga_x$ films prepared by combinatorial methods

2006 J. Phys.: Condens. Matter 18 4907

(http://iopscience.iop.org/0953-8984/18/20/015)

INSTITUTE OF PHYSICS PUBLISHING JOURNAL OF PHYSICS: CONDENSED MATTER

J. Phys.: Condens. Matter **18** (2006) 4907–4920 doi:10.1088/0953-8984/18/20/015

Mössbauer effect studies of $Fe_{100-x}Ga_x$ films prepared by combinatorial methods

R A Dunlap[1,2,3,4], N C Deschamps[1,2], R E Mar[2,3] and S P Farrell[1]

[1] Defence R&D Canada—Atlantic, PO Box 1012, Dartmouth, Nova Scotia, B2Y 3Z7, Canada
[2] Department of Physics and Atmospheric Science, Dalhousie University, Halifax, Nova Scotia, B3H 3J5, Canada
[3] Institute for Research in Materials, Dalhousie University, Halifax, Nova Scotia, B3H 3J5, Canada

E-mail: dunlap@fizz.phys.dal.ca

Received 22 December 2005, in final form 13 April 2006
Published 5 May 2006
Online at stacks.iop.org/JPhysCM/18/4907

Abstract

Magnetostrictive $Fe_{100-x}Ga_x$ alloys over the composition range $0 < x < 36$ have been prepared by combinatorial sputtering methods. These films were investigated by x-ray diffraction and ^{57}Fe Mössbauer effect spectroscopy techniques that have been adapted for the efficient study of combinatorial samples. X-ray diffraction measurements show the presence of a disordered bcc phase with a lattice parameter that increases with increasing Ga content. Mössbauer effect measurements show that even for low Ga content the disordered alloys are not truly random but show some degree of short range Ga clustering. For $x > 20$, the Mössbauer effect results suggest the presence of short range $D0_3$ type order. This persists up to the maximum Ga content studied here ($x = 36$), although there is no evidence to support the formation of long range $D0_3$ structural order in any of the films prepared in this study.

1. Introduction

Magnetostrictive materials change shape in the presence of a magnetic field and have a variety of potential applications as a result of these unusual magnetoelastic properties. Giant magnetostrictive materials such as Terfenol-D ($Tb_{1-x}Dy_xFe_2$) were discovered in the 1960s and have magnetostriction values of ~3600 ppm at room temperature. Although these materials have been widely used in actuators, sensors and energy harvesting devices, they tend to be expensive, brittle, and are not easily machined. Due to these limitations, non-rare-earth-based materials such as iron-based alloys are being studied for their desirable combination of toughness, formability and magnetostrictive properties. A promising magnetostrictive material is $Fe_{100-x}Ga_x$, also known as Galfenol. While Fe–Ga alloys do not yield as high a magnetostriction as Terfenol-D, other properties, such as ease of machining and higher tensile strength, make it attractive as a magnetostrictive material.

[4] Author to whom any correspondence should be addressed.

The magnetostrictive properties of $Fe_{100-x}Ga_x$ materials are highly dependent on composition, processing, preparation methods and thermal and stress history [1–6]. It is known that there is a close correlation between the crystallographic and grain structure of these alloys and their resulting magnetoelastic properties [1–7]. In particular, it is commonly believed that Ga–Ga pairing in alloys near $x = 19$ is responsible for an increase in magnetostriction and that the formation of an ordered $D0_3$ phase as the alloy composition approaches $x = 25$ is detrimental to this property [7]. Rapid quenching of these alloys influences both short and long range structural order as well as magnetic texture and has been investigated as a means of controlling the magnetoelastic properties. Although some work has been reported on quenching from the melt [8–10], little has appeared in the literature on thin film samples [11, 12].

Combinatorial sputtering [13] is an efficient and effective method of studying the composition dependence of alloys. Although many studies of Fe–Ga alloys have concentrated on fairly limited ranges of composition, combinatorial methods are ideal for investigation of materials over a large composition range. Various methods for the characterization and evaluation of materials have been adapted for the efficient study of combinatorial films. These include x-ray diffraction, electron microprobe and, in the case of Fe-containing materials, Mössbauer effect spectroscopy [14–16]. This latter technique has been shown [10, 15] to be particularly sensitive to microstructural details of the type that are believed to be important for magnetostrictive Fe–Ga. Often this occurs in cases where x-ray diffraction can provide relatively limited information. However, the use of Mössbauer effect spectroscopy for the study of Fe–Ga alloys has been relatively limited [10, 17–19].

In the present work we report on the preparation of $Fe_{100-x}Ga_x$ for $0 < x < 36$ by combinatorial sputtering methods. These samples are characterized by x-ray diffraction and ^{57}Fe Mössbauer effect spectroscopy with particular emphasis on the microstructure of the films. To our knowledge this represents the first report of Fe–Ga alloys prepared over a wide range of compositions by combinatorial methods.

2. Experimental methods

Three libraries of $Fe_{100-x}Ga_x$ covering the approximate composition ranges $2 < x < 17.5$ (library A), $14 < x < 24.5$ (library B) and $25.5 < x < 36$ (library C) were prepared by combinatorial sputtering methods. The sputtering machine consists of a modified Corona Vacuum Coaters model V-3T system. Substrates were placed on a circular rotating water-cooled table and the system contained an R2000 series Polycold cryopump to remove water vapour. The chamber was pumped during sputtering with a Varian TV-551 Navigator turbomolecular pump and the R2000 cryopump while argon was fed into the chamber to maintain a partial argon pressure of approximately 2 mTorr. Further details of the sputtering apparatus are available in the literature [13–16].

The sputtering targets used were Fe (AISI 1008 steel, 2N3 + Fe) and an $Fe_{50}Ga_{50}$ alloy. Compositions were controlled using aluminium masks [13]. A constant mask was used for the Fe target and a linear mask was used for the Fe–Ga target. For library A, a 0–100 'linear in' mask was used while for libraries B and C, a 50–100 'linear out' mask was used.

Various substrates of dimensions approximately 25 mm wide by 100 mm long were positioned on the sputtering table with the long axis placed radially on the table in order to produce several samples with identical composition ranges parallel to the long axis of the film. For the present study, films sputtered onto two (100) oriented Si wafers (for microprobe and x-ray measurements) and nine pieces of Kapton (for ^{57}Fe Mössbauer effect spectroscopy) were used. In addition, a series of aluminium weigh discs were positioned on the substrate table in order to monitor film thickness. Film thicknesses were typically around 0.8 μm.

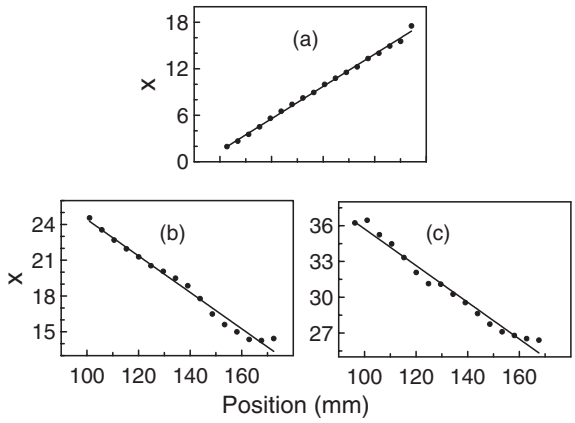

Figure 1. Composition of the three libraries as measured as a function of distance from the sputtering table axis: (a) library A, (b) library B and (c) library C. The inner edge of the sputtered film was approximately 95 mm from the table centre. Uncertainties are discussed in the text.

Compositions of the films were determined using a JEOL 8200 electron microprobe calibrated to a GaAs standard for Ga content.

X-ray diffraction patterns were obtained on two different diffractometers. An INEL CPS120 curved detector system was used for rapid x-ray diffraction measurements of the entire combinatorial film. The curved detector system measures all angles simultaneously in an area that is approximately 1 mm wide by 1 cm long. The detection width is always 1 mm since the angle of the x-rays to the surface of the sample remains at a constant shallow angle. A translation stage automatically moves the sample to order to obtain diffraction patterns as a function of position, and hence composition, along the length of the film.

The INEL system is useful for fast characterization of the crystal structure of the film as a function of composition. More accurate measurements of lattice parameters were obtained on a Philips X'Pert Pro diffractometer at selected film positions. All x-ray measurements were obtained at room temperature using Cu Kα radiation ($\lambda = 0.1542$ nm). The (400) reflection from the oriented Si substrate was an ideal internal standard.

Room temperature ^{57}Fe Mössbauer effect spectra were obtained using a $\underline{\text{Rh}}^{57}$Co source and a Wissel System II spectrometer operating in the constant acceleration mode. All spectra were referenced to room temperature α-Fe. In order to obtain sufficient thickness for Mössbauer effect measurements, nine layers of film deposited onto Kapton substrates were compositionally aligned and sandwiched together to form the absorber. The system incorporated a computer controlled translation stage that was synchronized to data collection to allow for the efficient investigation of the films. A spectrum of the film was accumulated through a slit aperture of 4.5 mm width at one position (composition) of the film. The film was then moved to the next position and a new spectrum initiated. The entire film was scanned in this manner. Data accumulation times at each position were typically 10–20 h. A detailed description of the translation stage setup is available in the literature [14–16].

3. Results

3.1. Microprobe results

Compositions measured by the microprobe as a function of position relative to the sputtering table axis are illustrated in figure 1. In all cases, an approximately linear change in composition

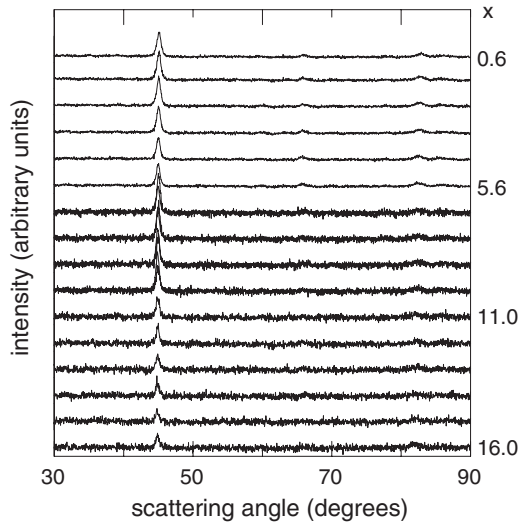

Figure 2. Room temperature Cu Kα x-ray diffraction patterns for library A as obtained with the INEL curved detector. Values of x are shown on the right-hand side for selected patterns.

is observed as a function of position. Typical composition uncertainties obtained from the microprobe were ± 1 at.%. In addition, uncertainty in correlating compositions between different pieces of substrate corresponded to an uncertainty of about ± 1 at.%. Thus, the alignment of data between libraries is accurate to about ± 2 at.%.

3.2. X-ray diffraction results

Room temperature x-ray diffraction measurements show all samples to be of the disordered bcc structure. An example of the results obtained from the INEL curved detector are illustrated (for library A) in figure 2. For these patterns, as well as all other x-ray and Mössbauer results, the quoted composition is the mean value of x over the portion of the film included in the measurement. No evidence was found in any of the x-ray measurements for the presence of superlattice peaks (principally around 26.5° and 55°) indicative of long range $D0_3$ type order. However, the very low intensity of these peaks makes their observation using x-ray diffraction very difficult. Measured lattice parameters of the bcc phase are shown in figure 3 along with values from the literature [6, 20]. These values follow the same general trend as those reported in the literature for alloys prepared by other methods. Our results are systematically slightly lower than those from the literature. This may be a real effect due to a difference in the sample preparation methods or it may merely be systematic instrumental differences.

3.3. Mössbauer effect results

Room temperature ^{57}Fe Mössbauer effect spectra for libraries A, B and C are shown in figures 4, 5 and 6, respectively. In view of the broadened lines observed in these spectra, as well as expectations concerning the structure of non-equilibrium processed alloys, these spectra were fitted to distributions of hyperfine parameters using Voigt-based functions, as has been commonly used for these types of material [21, 22]. In all cases a linear correlation between centre shift, δ, and the absolute value of the hyperfine field, $|H|$, of the form

$$\delta = \delta_0(x) + \delta_1(x)\,|H| \tag{1}$$

was assumed, where δ_0 and δ_1 are fitted parameters for each composition. For all fits presented here, the quadrupole shift was assumed to be zero as is expected for these materials. Fits where

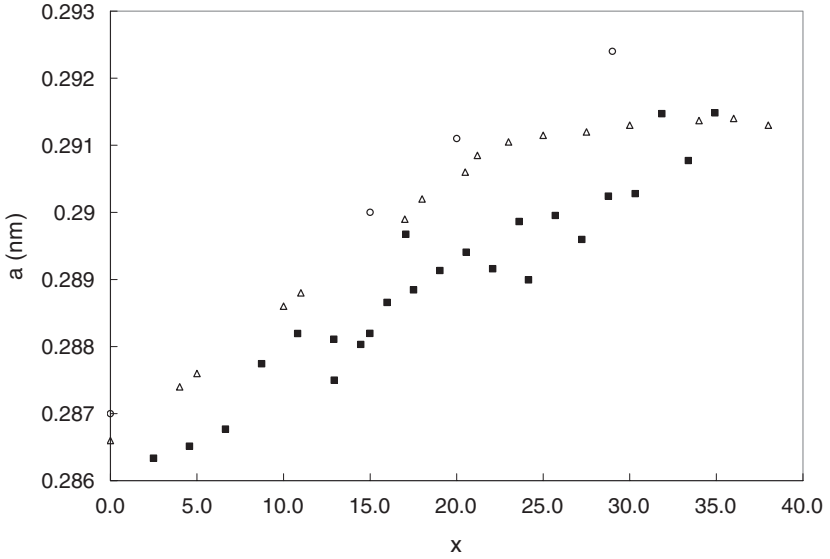

Figure 3. Lattice parameters, a, of $Fe_{100-x}Ga_x$ (■) as determined in this work and as reported in the literature by (△) Luo [19] and (○) Bormio-Nunes *et al* [6]. Typical uncertainties in our measurements are ±0.0005 nm.

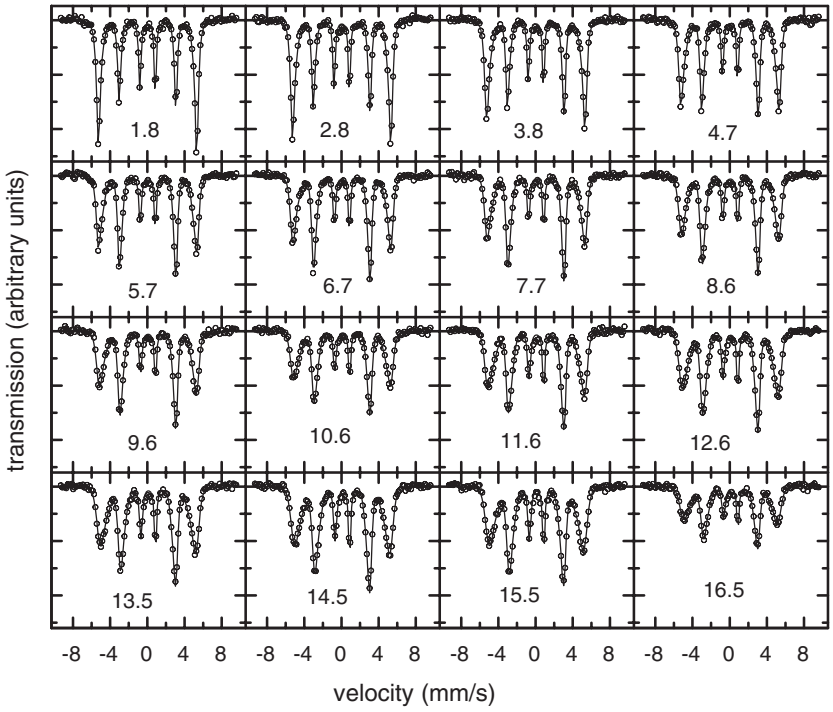

Figure 4. Room temperature ^{57}Fe Mössbauer effect spectra of library A of $Fe_{100-x}Ga_x$. The velocity scale is referenced to room temperature α-Fe. The value of x is shown for each spectrum. Solid lines are computer fits as described in the text.

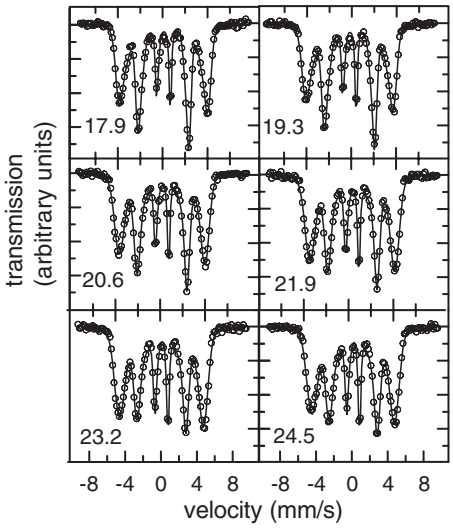

Figure 5. Room temperature ^{57}Fe Mössbauer effect spectra of library B of $Fe_{100-x}Ga_x$. The velocity scale is referenced to room temperature α-Fe. The value of x is shown for each spectrum. Solid lines are computer fits as described in the text.

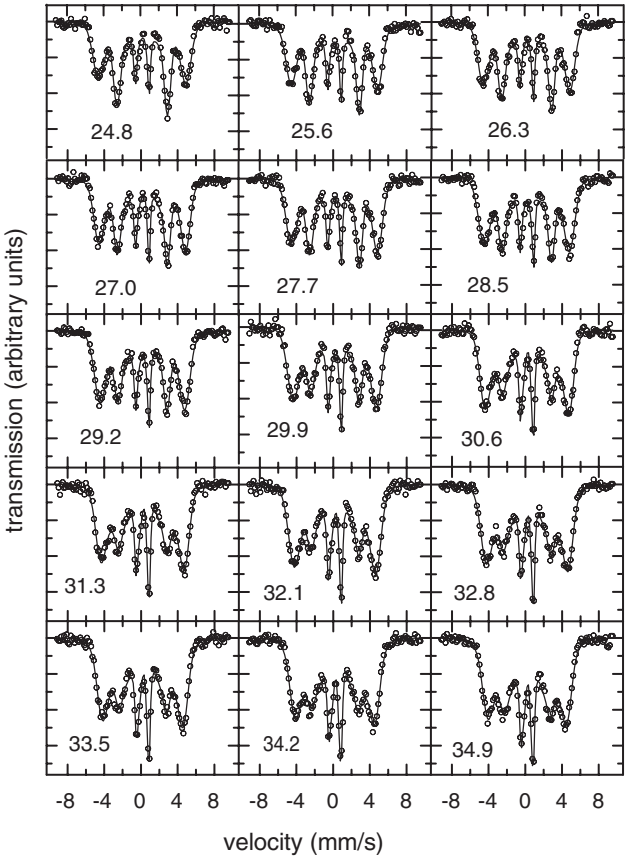

Figure 6. Room temperature ^{57}Fe Mössbauer effect spectra of library C of $Fe_{100-x}Ga_x$. The velocity scale is referenced to room temperature α-Fe. The value of x is shown for each spectrum. Solid lines are computer fits as described in the text.

this was a fitted parameter showed no evidence that this parameter was statistically non-zero. The Lorentzian line width was fixed at the value corresponding to the intrinsic spectrometer line width, 0.12 mm s^{-1} (HWHM). Hyperfine field distributions were expressed as combinations

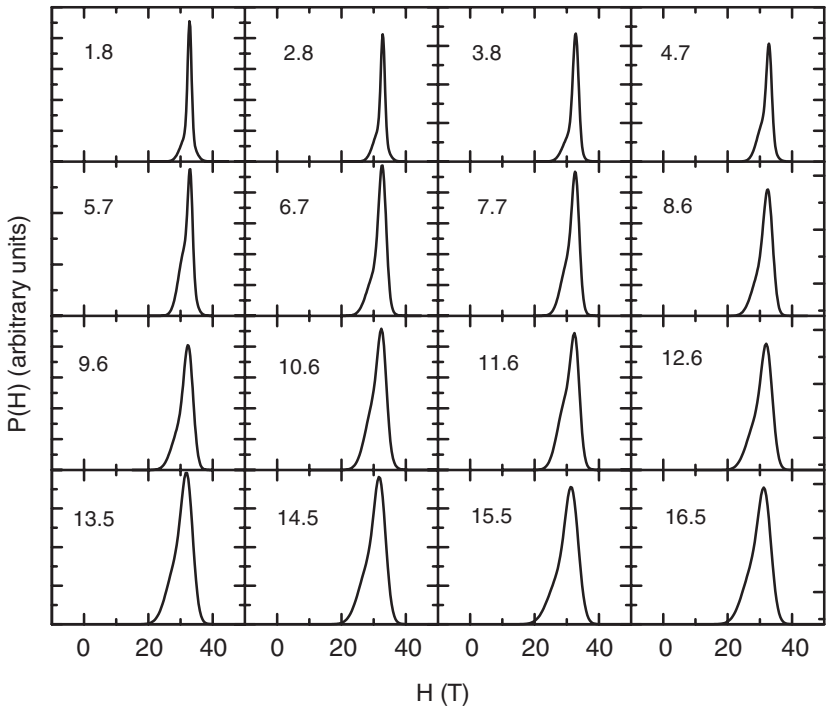

Figure 7. Room temperature ^{57}Fe hyperfine field distributions as obtained from two-component Voigt-based analysis of the Mössbauer effect spectra of library A of $Fe_{100-x}Ga_x$. The value of x is shown for each distribution.

of Gaussian distributed Lorentzians. Each Gaussian was characterized by a mean hyperfine field value, $\langle|H|\rangle$, and a width (standard deviation), σ. For each spectrum all Gaussians had common values of δ_0, δ_1 and Lorentzian line intensity ratios, $A_1{:}A_2{:}A_3{:}A_3{:}A_2{:}A_1$. Fits where these were independent parameters for each Gaussian did not provide substantially improved fits or additional physical insight into the properties of the films. The criteria for determining the most reasonable number of components in the hyperfine field distribution has been discussed by Dunlap and co-workers [10, 23]. The most reasonable fit was determined by the location of the knee in a plot of the goodness-of-fit versus degrees of freedom as well as an analysis of the relevance of features in the overall hyperfine field distribution. The present analysis indicates that two Gaussian components in the hyperfine field distribution are appropriate for spectra across the entire range of compositions studied here. These components are distinguished on the basis of their mean hyperfine field and are subsequently referred to as high-field and low-field components. The fitted curves are shown in figures 4–6 and the resulting hyperfine field distributions are shown in figures 7–9. Fitted hyperfine parameters as a function of alloy composition are shown in figures 10–14.

The centre shift as seen in figure 10 exhibits a reasonably linear trend to more positive values with increasing Ga content. At the low Ga end, the values extrapolate to close to the pure Fe value and values from the three libraries align quite well at their end points: at around $x = 17$ and 25. The minor discrepancies exhibited by the centre shift as a function of composition are within expectations based on uncertainties in the compositions and minor deviations from compositional linearity that occur near the ends of the films as seen in figure 1. The consistency of the results obtained here are typical of those obtained from other studies

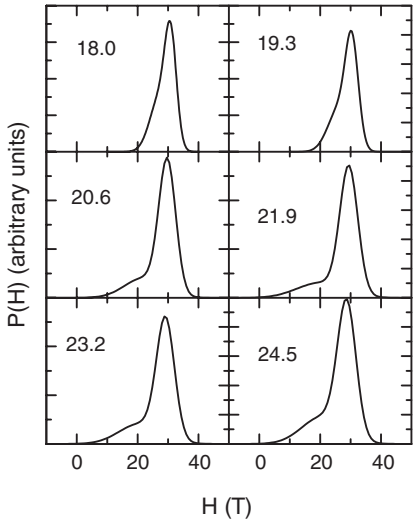

Figure 8. Room temperature ^{57}Fe hyperfine field distributions as obtained from two-component Voigt-based analysis of the Mössbauer effect spectra of library B of $Fe_{100-x}Ga_x$. The value of x is shown for each distribution.

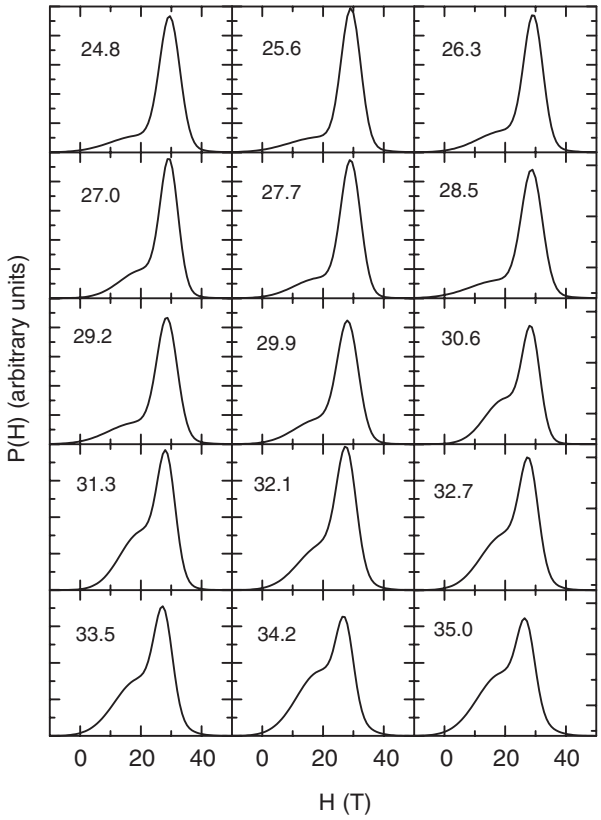

Figure 9. Room temperature ^{57}Fe hyperfine field distributions as obtained from two-component Voigt-based analysis of the Mössbauer effect spectra of library C of $Fe_{100-x}Ga_x$. The value of x is shown for each distribution.

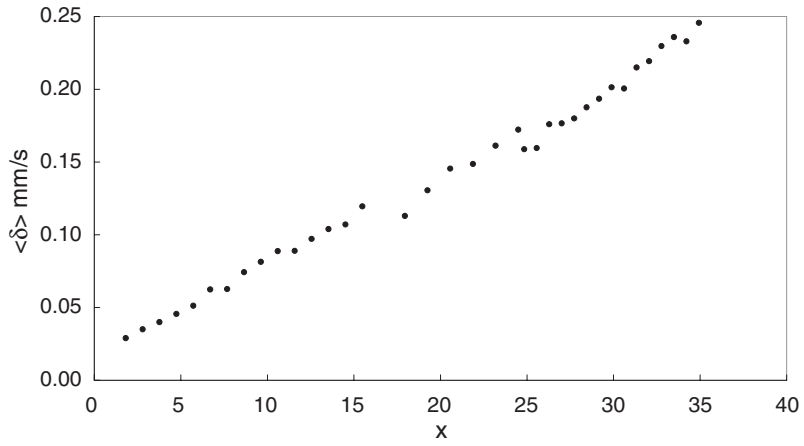

Figure 10. Mean centre shift, $\langle\delta\rangle$, of $Fe_{100-x}Ga_x$ films as a function of x. Typical uncertainties are ± 0.005 mm s^{-1}.

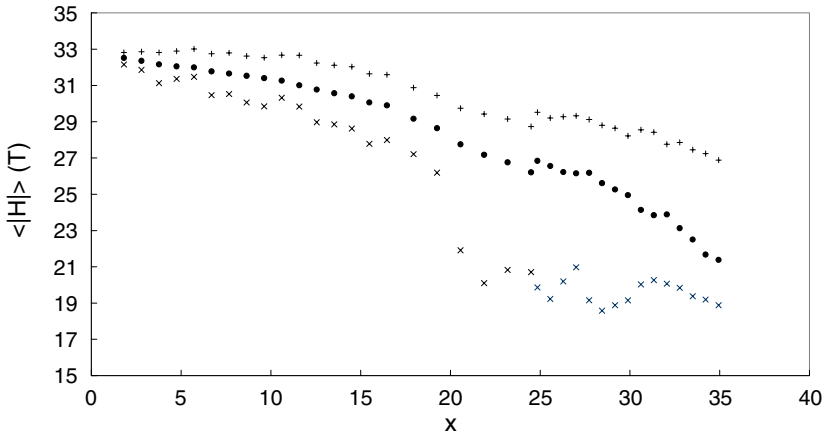

Figure 11. Mean Fe hyperfine field, $\langle|H|\rangle$, of $Fe_{100-x}Ga_x$ as a function of x; (+) high-field component, (×) low-field component and (●) total distribution. Typical uncertainties are ±0.5 T. (This figure is in colour only in the electronic version)

involving multiple combinatorial libraries [15] and may be used as a basis for the interpretation of the other Mössbauer effect parameters reported below.

The mean values of the hyperfine fields of the two components illustrated in figure 11 show a decrease with increasing Ga content. This is expected for the Fe field in a bcc structure diluted with non-magnetic Ga ions. While the mean of the total distribution shows a relatively smooth decrease across the entire range of compositions, the mean fields associated with the two individual field components both show smaller changes in the field as a function of composition above about $x = 20$. This is most obvious in the behaviour of the low-field component and the behaviour of the mean of the total distribution in this region results to a large extent from the changing proportions of the two components rather than the change associated with the mean fields of the components. This is discussed further with regard to figure 14.

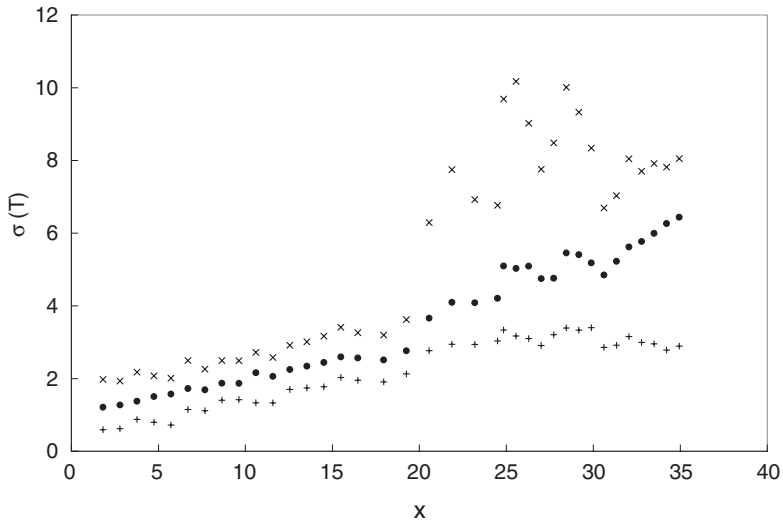

Figure 12. Gaussian width, σ, of the hyperfine field distribution of $Fe_{100-x}Ga_x$ as a function of x; (+) high-field component, (×) low-field component and (●) total distribution. Typical uncertainties are ±0.2 T.

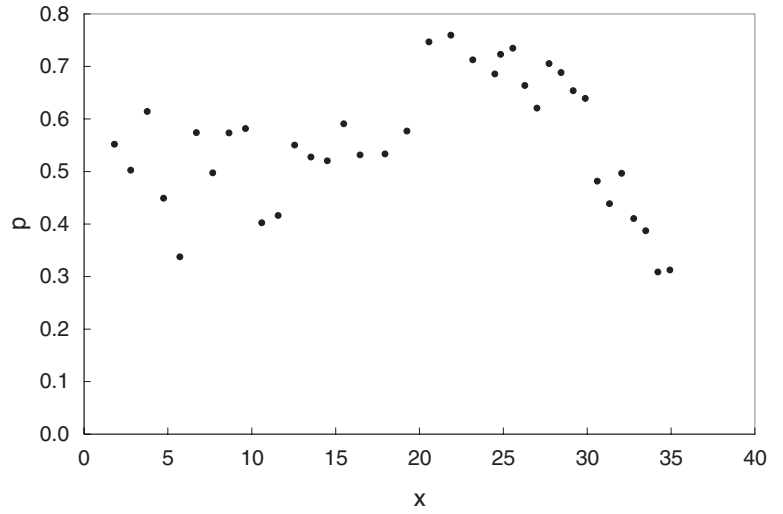

Figure 13. Relative intensity, p, of the high-field component of the hyperfine field distribution of $Fe_{100-x}Ga_x$ as a function of x. Typical uncertainties are ±0.05.

The Gaussian widths, as shown in figure 12, increase with increasing Ga content. This is expected for a disordered alloy as the concentration of the substituted atoms increases due to the increase in the diversity of Fe probe atom environments. Perhaps the most striking feature of this figure is the substantial increase in the width of the low-field component for $x > 20$.

The relative intensity of the high-field spectral component, p, is shown in figure 13. Although there is substantial scatter in the data, there is some suggestion that p remains more or less constant around 0.5 for x up to about 20, followed by a fairly sharp increase and then a gradual decrease. It is, perhaps, relevant that the sharp increase occurs towards the end of library B and is not associated with the transition between libraries.

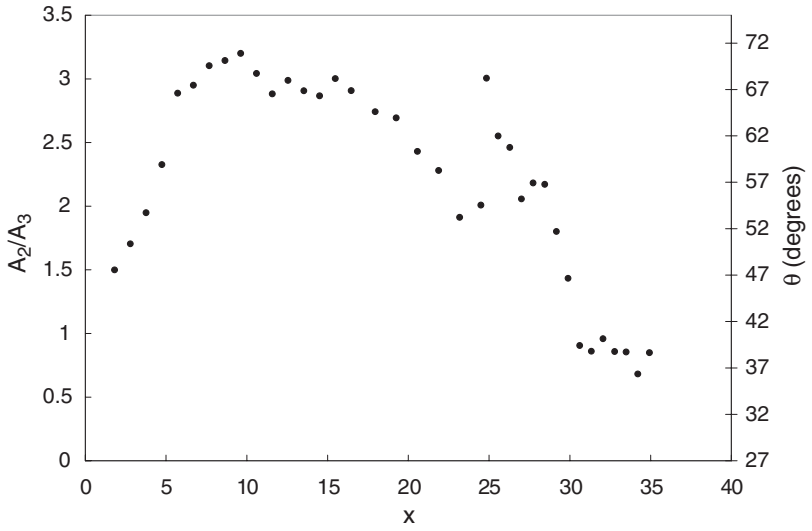

Figure 14. Intensity ratio A_2/A_3 for $Fe_{100-x}Ga_x$ thin films as a function of x. Typical uncertainties are ± 0.1. Calculated angles between the magnetization direction and the incident γ-ray direction, θ, are shown by the scale on the right-hand side of the graph.

The ratio of line intensities A_1/A_3 has been a free fitting parameter in all fits. The value of this ratio for all spectra was 3.1 ± 0.2, consistent with the theoretical value of 3.0. This supports the validity of the analysis and the interpretation of the other hyperfine parameters.

The values of A_2/A_3 are illustrated in figure 14. These show a clear variation as a function of x. In general, this corresponds to an increase up to about $x = 8$ followed by a decrease with some anomalous behaviour around $x = 27$. This region corresponds to the end of library C and it is possible that differences in sputtering conditions near the end of the film may be a factor for these data. The ratio A_2/A_3 is determined by the relative orientation of the incident γ-ray and the principal axis of the magnetization (the angle θ). This ratio varies between 0 (for $\theta = 0°$; corresponding to a magnetization perpendicular to the film) to 4 (for $\theta = 90°$; corresponding to a magnetization in the plane of the film). The angle θ is determined from the intensities A_2 and A_3 by [24]

$$\theta = \sin^{-1}\left[\sqrt{\frac{2A_2}{A_2 + 4A_3}}\right]. \tag{2}$$

These values are also shown in the figure. Changes in magnetic texturing of the films are clearly indicated by these results.

4. Discussion and conclusions

The x-ray measurements reported are consistent with the basic bcc structure of the alloys for all compositions and have provided lattice parameters consistent with literature values. X-ray diffraction measurements provide little information about the details of the chemical ordering in this phase due to the low intensity of the $D0_3$ superlattice reflections and the general insensitivity of x-ray diffraction to short range chemical order. Mössbauer effect spectroscopy, however, is sensitive to the local environment around the Fe probe atoms and is an ideal technique for investigating the types of short range structural ordering that is suspected of

playing an important role in the determination of the magnetoelastic properties of Fe–Ga. The Mössbauer effect results reported here are the first for combinatorially prepared libraries of the Fe–Ga system. However, the present study may be considered in the context of previous Mössbauer effect results reported in the literature for Fe–Ga prepared by other methods.

Wertheim *et al* [19] have undertaken an analysis of the Mössbauer effect spectra of $Fe_{100-x}Ga_x$ on the basis of the first and second nearest neighbour Ga coordination around the Fe probe site. Newkirk and Tsuei [18] have taken the same approach, and using a more detailed analysis over a wider composition range have identified spectral components associated with differing numbers of Ga neighbours. Kawamiya *et al* [17] have concentrated on a limited composition range around $x = 25$ and have considered the local Fe environment in the context of bcc, $D0_3$ and $L1_2$ ordering. Dunlap *et al* [10] have looked at melt spun samples with compositions between $x = 8.3$ and 23.3 and have suggested the existence of a disordered bcc phase with Ga pairing up to about $x = 20$ and short range $D0_3$ ordering for higher Ga content.

The centre shifts shown in figure 10 increase with increasing Ga content at a rate of 0.0065 mm s^{-1} per at.% Ga. This is consistent with the increase in the mean value of the centre shift reported by Newkirk and Tsuei [18] which increases with Ga content at a rate of 0.0061 mm s^{-1} per at.% Ga. Quantitatively this change in centre shift can be explained in terms of the electronic structure of Fe and Ga. The substitution of Ga ($[Ar]3d^{10}4s^23p^1$) for Fe ($[Ar]3d^64s^2$) increases the total number of d electrons. This increases the shielding of the 4s electrons at the Fe nucleus, leading to a decrease in the electron density at the probe nucleus and a correspondingly more positive centre shift.

The decrease in hyperfine fields as a function of Ga content shown in figure 11 is consistent with the mean fields reported by Newkirk and Tsuei [18]. A direct comparison of the changes in Fe hyperfine field as a function of Ga content between the present results and those of Newkirk and Tsuei [18] is not straightforward. This is a consequence of the different fitting philosophies as well as the somewhat non-linear changes in the fields, although both studies show a similar decrease in mean field of about 0.15 T per at.% Ga for small Ga concentrations. Discrete spectral components corresponding to specific Ga nearest and second nearest neighbour coordination around the Fe probe sites as observed by Newkirk and Tsuei [18] are not seen in the present spectra. This is presumably due to the disordered nature of the samples resulting from the sputtering process. However, an analysis of the relationship of hyperfine field and Ga coordination as reported by Newkirk and Tsuei [18] shows that there is a fairly well defined distinction between hyperfine field values for Fe with zero or one Ga nearest neighbour and those for Fe with two or more Ga nearest neighbours. These categories of Fe sites correspond to the high-field and low-field components, respectively, in the present spectral analysis. This same distinction has been seen by Dunlap *et al* [10] for melt spun Fe–Ga alloys, at least up to about 20 at.% Ga.

The relatively small change in Fe hyperfine fields as a function of Ga content for x greater than about 20 may be viewed in the context of results of Kawamiya *et al* [17] and Dunlap *et al* [10]. Between about $x = 22$ and 28, figure 11 shows that the two hyperfine field components remain more or less constant as a function of Ga content at about 29 T (for the high-field component) and 20 T (for the low-field component). These two field components have been identified in the spectrum of an $x = 23.3$ melt spun sample by Dunlap *et al* [10]. These components correspond to the two sites present in the ordered $D0_3$ phase as reported by Kawamiya *et al* [17] for well-ordered samples with x near 25. Consistent with Dunlap *et al* [10] the present measurements show the prevalence for local $D0_3$ ordering in Fe–Ga alloys as x approaches 25. This is possibly due to the formation of ⟨110⟩ Ga–Ga pairs for alloys with compositions near the stoichiometric $D0_3$ composition ($x = 25$). The field distributions are not

as well defined as those observed by Dunlap *et al* [10] for melt spun alloys, presumably as a result of the greater degree of disorder present in the sputtered samples. This may specifically be the result of the range over which Ga–Ga pairing remains correlated. For greater than about 28 at.% Ga the data suggest a slight decreasing trend in the fields associated with the two components. This may result from Ga in excess of the stoichiometric $D0_3$ amount increasing the probability of larger Ga clusters.

As is seen in figure 12, the low-field component, corresponding to Fe with two or more Ga neighbours, shows a greater Gaussian width than that for the high-field component for all Ga concentrations. This difference in Gaussian widths is most obvious above about $x = 20$. In the nearest neighbour shell, the diversity of Fe environments for Fe sites with zero or one Ga neighbour is limited. However, for two or more neighbour Ga the variations in Fe environments is greater and this diversity increases as the Ga content increases.

The relative proportions of the high-field and low-field components, p, as shown in figure 13, provide information about the short range order in these samples. For disordered bcc samples with randomly distributed Ga the value of p should decrease monotonically from a value of $p = 1$ at $x = 0$ with increasing Ga content. The present results clearly indicate that this behaviour is not observed. In general, the low values of p for small x indicate that there is an excess number of Fe sites with more Ga neighbours than statistically expected. This same feature has been observed in melt spun Fe–Ga up to about $x = 20$ [10]. The specific distribution of Ga neighbours cannot be established on the basis of the value of p. However, Lograsso *et al* [7] have suggested that the large magnetostriction observed in the Fe–Ga system may be explained by the tendency of Ga atoms to pair along the ⟨100⟩ directions. Although the overall effect of ⟨100⟩ pairing on the value of p in a disordered system is not obvious, this type of pairing will increase the proportion of Fe sites with two Ga nearest neighbours at the expense of Fe sites with one Ga nearest neighbour and may be consistent with the present Mössbauer results. The increase in p above $x = 20$ suggests increased Ga pairing along the ⟨110⟩ Ga direction as a precursor to short range $D0_3$ phase formation as x approaches 25. For x greater than about 28 or 30, the value of p decreases due to the statistical probability for the formation of larger Ga clusters. Details of Ga distributions in these alloys have been illustrated in figures 5 and 6 of [10].

A final observation may be made concerning the magnetization orientation as illustrated in figure 14. For a randomly magnetized sample the value of A_2/A_3 is 2.0. The present results indicate the presence of magnetic texture where the principal magnetization axis tends to point out of the plane of the film for small and large x but tends to lie more in the plane of the film for x in the range of about 5–20. This feature may be coupled to the fundamental magnetoelastic properties of the alloys as a function of Ga content. On the other hand, differences in sputtering conditions, substrate lattice spacing, film thickness, etc as a function of position on the film may play a role. The latter is suggested as a possible contributing factor by the anomalous features that appear at the transition between libraries B and C. However, the consistency of the results between libraries A and B suggests the importance of a more fundamental dependence on Ga composition. Further studies of these effects are necessary to clarify the reasons for the details of magnetic texture illustrated in figure 14.

The present investigation has demonstrated the usefulness of combinatorial methods for studying the composition dependence of the properties of alloy systems over a wide composition range. In particular, the present study represents the first application of these techniques to the Fe–Ga system. We have also demonstrated the ability to adapt structural and magnetic characterization methods, specifically x-ray diffraction and Mössbauer effect spectroscopy, for the efficient study of combinatorial films. The ability of Mössbauer spectroscopy to identify details of the microstructure that are difficult or impossible to observe

using x-ray diffraction techniques has been demonstrated in this study. In addition, information about short range order and atomic clustering can be obtained. The present investigations have shown that the distribution of Ga atoms within the bcc phase is not random and that the disordered bcc phase that is observed in x-ray studies is, in fact, characterized by clustering of Ga atoms. This clustering has been shown, both in the present study and in our previous work on melt spun samples [10], to occur as a precursor to $D0_3$ ordering and is consistent with the common understanding (e.g. [7]) that such short range order is an important factor in determining the magnetoelastic properties of Fe–Ga alloys.

Acknowledgments

This work was funded by the Natural Sciences and Engineering Research Council of Canada, the Killam Trusts and Defence R&D Canada. The authors are grateful to J R Dahn, G Fisher, J D McGraw, P Stoffyn and J Lawless for their contributions to this work.

References

[1] Clark A E, Restorff J B, Wun-Fogle M, Lograsso T A and Schlagel D L 2000 *IEEE Trans. Magn.* **36** 3238
[2] Srisukhumbowornchai N and Guruswamy S 2002 *J. Appl. Phys.* **92** 5371
[3] Srisukhumbowornchai N and Guruswamy S 2001 *J. Appl. Phys.* **90** 5680
[4] Clark A E, Hathaway K B, Wun-Fogle M, Restorff J B, Lograsso T A, Keppens V M, Petculescu G and Taylor R A 2003 *J. Appl. Phys.* **93** 8621
[5] Cullen J R, Clark A E, Wun-Fogle M, Restorff J B and Lograsso T A 2001 *J. Magn. Magn. Mater.* **226–230** 948
[6] Bormio-Nunes C, Tirelli M A, Sato Turtelli R, Grössinger R, Müller H, Wiesinger G, Sassik H and Reisser M 2005 *J. Appl. Phys.* **97** 033901
[7] Lograsso T A, Ross A R, Schlagel D L, Clark A E and Wun-Fogle W 2003 *J. Alloys Compounds* **350** 95
[8] Clark A E, Wun-Fogle M, Restorff J B, Lograsso T A and Cullen J R 2001 *IEEE Trans. Magn.* **37** 2678
[9] Cheng S F, Das B N, Wun-Fogle M, Lubitz P and Clark A E 2002 *IEEE Trans. Magn.* **38** 2838
[10] Dunlap R A, McGraw J D and Farrell S P 2006 *J. Magn. Magn. Mater.* at press
[11] Butera A, Weston J L and Barnard J A 2004 *J. Magn. Magn. Mater.* **284** 17
[12] Weston J L, Butera A, Lograsso T, Shamsuzzoha M, Zana I, Zangari G and Barnard J 2002 *IEEE Trans. Magn.* **38** 2832
[13] Dahn J R, Trussler S, Hatchard T D, Bonakdarpour A, Mueller-Neuhaus J R, Hewitt K C and Fleischauer M D 2002 *Chem. Mater.* **14** 3519
[14] Fleischauer M D, Obrovac M N, McGraw J D, Dunlap R A, Topple J M and Dahn J R 2006 *J. Electrochem. Soc.* **153** A484
[15] McGraw J D, Fleischauer M D, Dahn J R and Dunlap R A 2006 *Phil. Mag.* at press
[16] McGraw J D, Fleischauer M D, Dahn J R and Dunlap R A 2005 *Proc. 11th CF/DRDC Int. Mtg on Naval Applications of Materials Technology (Dartmouth)* p 266
[17] Kawamiya N, Adachi K and Nakamura Y 1972 *J. Phys. Soc. Japan* **33** 1318
[18] Newkirk L R and Tsuei C C 1971 *Phys. Rev.* B **4** 4046
[19] Wertheim G K, Jaccarino V, Wernick J H and Buchanan D N E 1964 *Phys. Rev. Lett.* **12** 24
[20] Luo H L 1967 *Trans. Metall. Soc. AIME* **239** 119
[21] Legarec K and Rancourt D G 1997 *Nucl. Instrum. Methods* B **129** 266
[22] Rancourt D G and Ping J Y 1991 *Nucl. Instrum. Methods* B **58** 85
[23] Dunlap R A and Ritcey S P 1985 *Phys. Rev.* B **32** 3325
[24] Greenwood N N and Gibb T C 1971 *Mössbauer Spectroscopy* (London: Chapman and Hall) pp 66–72